



Research article

Apostolos Zdagkas, Nikitas Papasimakis*, Vassili Savinov, Mark R. Dennis
and Nikolay I. Zheludev

Singularities in the flying electromagnetic doughnuts

<https://doi.org/10.1515/nanoph-2019-0101>

Received April 3, 2019; revised May 28, 2019; accepted May 29, 2019

Abstract: Flying doughnuts (FDs) are exact propagating solutions of Maxwell equations in the form of single-cycle, space-time non-separable toroidal pulses. Here we review their properties and reveal the existence of a complex and robust fine topological structure. In particular, the electric and magnetic fields of the FD pulse vanish across a number of planes, spherical shells and rings, and display a number of point singularities including saddle points and vortices. Moreover, the instantaneous Poynting vector of the field exhibits a large number of singularities, which are often accompanied by extended areas energy backflow.

Keywords: toroidal pulse; toroidal electrodynamics; flying doughnut; topology; vortex; singularities.

1 Introduction

Vortex rings in fluid flows have long been a source of fascination: they are localized, axisymmetric disturbances which carry linear momentum through the medium [1]. This behavior is understood by a combination of the topology of toroidal flow around a closed ring with the physics of fluid flow around a curved vortex, which guarantees the uniform forward motion of the ring. Here, we describe the

topology underlying an electromagnetic analogue of fluid vortex rings, the so-called flying doughnut pulses (FD) [2]. These are time-dependent, axially symmetric single-cycle toroidal disturbances propagating at lightspeed along the axis of the torus. The FD fields we study follow an envelope of a focused Gaussian beam; nevertheless, we show how the vectorial structure of the FD fields, consisting of the electric field, magnetic field and Poynting vector, can be understood in terms of their topology, in particular in terms of the instantaneous, real vector field zeros which form circulations, saddle points as well as sources and sinks in two-dimensional slices of the three-dimensional cylindrically symmetric fields. This description of the electromagnetic field topology is appropriate for FD fields which are pulses, rather than polarization singularities (e.g. C lines, L surfaces on which the polarization is circular and linear, respectively [3–7]) in monochromatic fields. Indeed, FD pulses are so short that polarization ellipses cannot be naturally defined in these fields, nor even can other, broadband descriptions of electric and magnetic field behavior such as Lissajous curves [8, 9]. The vector field structures we study, nevertheless, are field zeros which form a topological skeleton providing a complete description of the anatomy of FD fields.

FDs are single-cycle pulses of toroidal topology, where the electric and magnetic fields are mainly confined on the surface and volume of a torus, respectively. In contrast to the typically encountered transverse waves, this field configuration leads to longitudinal field components that are oriented along the direction of pulse propagation (see Figure 1A). FD pulses belong to a wider family of exact solutions to Maxwell's equations that were introduced by Brittingham and Ziolkowski [10–12] in the context of non-diffracting waves (focus wave modes), in which the spatial and temporal dependence cannot be separated. However, FDs can be focused and diffract without distortion similarly to monochromatic Gaussian beams. FD pulses can be distinguished in transverse electric (TE) and transverse magnetic (TM). In cylindrical coordinates (ρ, θ, z) , the electric and magnetic fields of the TE FD pulse coming to focus at $t=0, z=0$ are given by [2]

*Corresponding author: Nikitas Papasimakis, Optoelectronics Research Centre, University of Southampton, Southampton SO17 1BJ, UK, e-mail: n.papasimakis@soton.ac.uk.

<https://orcid.org/0000-0002-6347-6466>

Apostolos Zdagkas and Vassili Savinov: Centre for Photonic Metamaterials and Optoelectronics Research Centre, Zepler Institute, University of Southampton, Southampton SO17 1BJ, UK

Mark R. Dennis: School of Physics and Astronomy, University of Birmingham, Birmingham B15 2TT, UK

Nikolay I. Zheludev: Optoelectronics Research Centre, University of Southampton, Southampton SO17 1BJ, UK; and Centre for Disruptive Photonic Technologies, School of Physical and Mathematical Sciences & The Photonics Institute, Nanyang Technological University, 637371 Singapore

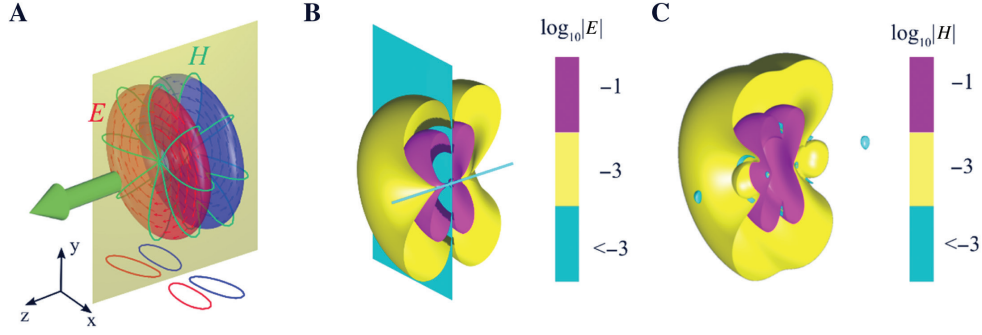


Figure 1: Large- and fine-scale topology of the single-cycle TE FD pulse.

(A) Iso-surface of the electric field consisting of two doughnut-shaped regions. Red and blue colors indicate the two half-cycles of the pulse, respectively. Green lines show the (radially and longitudinally oriented) magnetic field winding around the (azimuthally oriented) electric field, while red arrows mark the direction of the latter. The solid green arrow indicates the direction of pulse propagation along the positive z -axis. (B, C) Iso-surface plots of the logarithm of the normalized electric (B) and magnetic (C) field modulus at different field values. Purple color marks the strong field central regions of the pulse presented in (A), while light blue indicates the location of the zeros of the fields. In order to reveal the complex field structure, only the half of the pulse that lies in the negative x -space is presented in (B) and (C). In all panels, the pulse is considered at focus ($t=0$), while $q_2=10q_1$.

$$\begin{aligned} \vec{E} &= E_\theta \hat{\theta} = -4if_0 \sqrt{\frac{\mu_0}{\varepsilon_0}} \frac{\rho(q_1 + q_2 - 2ict)}{[\rho^2 + (q_1 + i\tau)(q_2 - i\sigma)]^3} \hat{\theta} \\ \vec{H} &= H_\rho \hat{\rho} + H_z \hat{z} = 4f_0 \left[i \frac{\rho(q_2 - q_1 - 2iz)}{[\rho^2 + (q_1 + i\tau)(q_2 - i\sigma)]^3} \hat{\rho} \right. \\ &\quad \left. - \frac{\rho^2 - (q_1 + i\tau)(q_2 - i\sigma)}{[\rho^2 + (q_1 + i\tau)(q_2 - i\sigma)]^3} \hat{z} \right], \end{aligned} \quad (1)$$

where $\sigma = z + ct$, $\tau = z - ct$, and q_1, q_2 play the role of the effective wavelength and Rayleigh range, respectively. In particular, the value of the ratio q_2/q_1 indicates whether the pulse is collimated ($q_2/q_1 \gg 1$) or strongly focused. The electric field is azimuthally polarized with no longitudinal or radial components, whereas the magnetic field is oriented along the radial and longitudinal directions with no azimuthal component (see Figure 1A). The TM FD pulse can be obtained by an exchange of electric and magnetic fields [2]. From the complex electromagnetic fields of Eq. (1), two different pulses can be constructed corresponding to the real and imaginary parts of the fields, respectively. Both types of pulses are exact solutions to Maxwell's equations. The real part corresponds to a pulse, which is single-cycle in the electric field and $1\frac{1}{2}$ -cycle in the magnetic field, whereas the imaginary part leads to a pulse, which is $1\frac{1}{2}$ -cycle in the electric field and single-cycle in the magnetic field. We refer to the real part as the single-cycle pulse and to the imaginary part as the $1\frac{1}{2}$ -cycle pulse. Upon propagation, single-cycle ($1\frac{1}{2}$ -cycle) transforms to the $1\frac{1}{2}$ -cycle (single-cycle) pulse due to the Gouy phase shift [13].

The presence of both longitudinal and transverse field components has led to suggestions for applications, such as charged particle acceleration [2], whereas even

simple properties of the pulse, such as interactions with dielectric and metallic interfaces, can be nontrivial [14]. In particular, while the fields of the TE pulse retain their orientation relative to the propagation direction upon reflection, this is not true for the TM pulse. The latter acquires a longitudinal field antiparallel to its propagation direction when it is reflected from a perfect electric conductor or a dielectric interface. These field transformations are direct consequence of the boundary conditions at the interface in combination with the complex topology of the pulse. Importantly, the doughnut-like configuration of electric and magnetic fields is topologically similar to that of the recently discovered toroidal dipole excitations, and in fact it has been shown that FD pulses are promising candidates for exciting toroidal modes and non-radiating configurations in matter [15, 16]. This has been demonstrated through the interaction of the FD pulse with spherical dielectric non-dispersive nanoparticles. The multipole expansion of the radiated field was used to show that a strong toroidal moment is induced despite the fact that the particle does not possess toroidal symmetry. In addition, the cross term in the scattered intensity between the toroidal and dipole moment showed that the two modes interfere destructively and overall lead to the excitation of a dynamic anapole, which manifests as a dip in the total scattering intensity at the corresponding resonance frequency. Recently, a scheme for the generation of FDs based on spatially and temporally dispersive metasurfaces was put forward, and efforts for experimental characterization of such pulses are underway [17, 18].

Here we investigate the topological properties of FD pulses in terms of the singular points, that is, the real

vector field zeros of the pulse, where either the electric field or magnetic field, and the Poynting vector vanish. We demonstrate that in contrast to the relatively simple toroidal shape presented by the high intensity areas of the pulse (see Figure 1A), a complex structure of electric and magnetic field vortices, as well as energy backflow, is revealed at the lower energy scales (Figure 1B and C). Our study focuses on the single-cycle (real) and $1/2$ -cycle (imaginary) TE pulse; however, our conclusions hold for the TM case as well (by exchanging electric and magnetic fields). Moreover, in the following we choose a small value of the Rayleigh range $q_2 = 20q_1$, which places our study in the non-paraxial regime and allows us to investigate all singular points of the pulse in a relatively small region.

2 Electric field singularities

The instantaneous electric field for the single-cycle TE FD pulse is presented in Figure 2 for $t=0$, when the pulse comes into focus. Owing to its azimuthal polarization, the electric field vanishes along the propagation axis ($\rho=0$) similarly to the phase singularities observed in vector polarized monochromatic beams [7] (see the vertical solid black line in Figure 2A). The electric field also vanishes in the $z=0$ plane (see the horizontal solid black line in Figure 2B) due to the single-cycle nature of the pulse, which implies odd symmetry for the electric field upon reflection across the x -axis (at $t=0$). In contrast to the simple two-lobe picture presented in Figure 1A,

the electric field presents a complex behavior, where it vanishes on two spherical shells (indicated by the solid circles in the left panel of Figure 2) on the positive and negative z -axis, respectively. This behavior can be more clearly observed in Figure 2A–C, where cross-sections normal to the propagation axis are presented. In accordance to Figure 1A, the electric field close to and away from the center of the pulse (cross-sections A and C) rotates counter-clockwise forming a vortex around the singularity along the propagation axis. However, at a distance of $\sim 5q_1$ from its center ($z=0$), the electric field vanishes on a circular boundary, which corresponds to a spherical region inside which the electric field is oriented along the clockwise direction, whereas outside this region the electric field remains oriented in the opposite (counter-clockwise) direction (see cross-section B).

A similar behavior is displayed by the $1/2$ -cycle pulse (see Figure 3), where the electric field also vanishes along the propagation axis. However, in contrast to the single-cycle pulse of Figure 2, the electric field here does not vanish on the $z=0$ plane; rather it is at a maximum in this region as a result of its $1/2$ -cycle nature, which leads to even symmetry of the electric field at $t=0$ (see the left panel in Figure 3). As in the case of the single-cycle pulse, the electric field is zero on two spherical shells on positive and negative z , respectively, which separate regions with opposite directions of the electric field. Indeed, the electric field vortex around the propagation axis changes the direction of its rotation, from counter-clockwise at $z=0$ to clockwise inside the spherical regions within the circular singularities, to counterclockwise again at large values

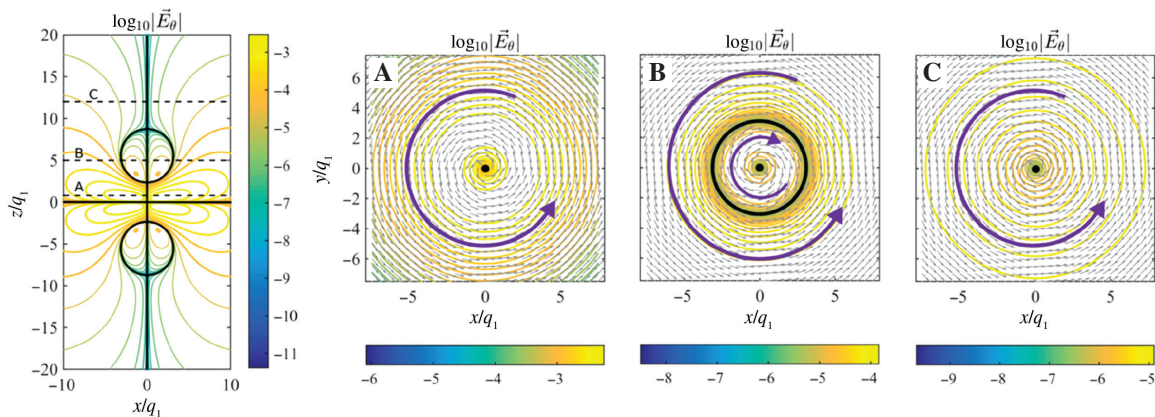


Figure 2: Electric field topology of the single-cycle TE FD pulse at focus.

The left panel presents an isoline plot of the logarithm of the electric field in the xz plane. Solid black lines indicate the zeros of the electric field. Dashed lines marked as A–C indicate the z -levels of the cross-sections on the three right panels. Panels (A)–(C) present isoline plots of the logarithm of the electric field and arrow plots of the electric field direction in the xy plane. Solid black lines and black dots mark the points and areas, where the electric field vanishes. Purple arrows indicate the direction of the electric field and serve as guide to the eye. The pulse is at focus ($t=0$) and propagates along the positive z -axis.

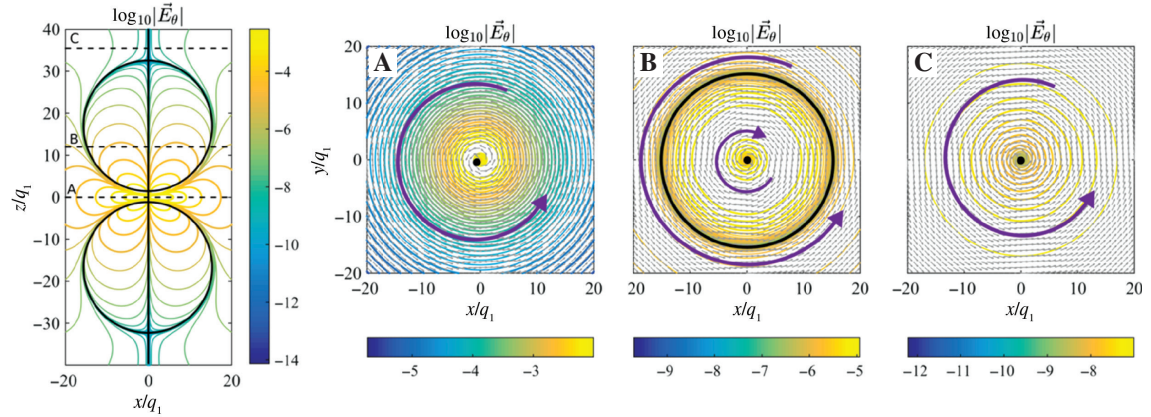


Figure 3: Electric field topology of the $1/2$ -cycle TE FD pulse at focus.

The left panel presents an isoline plot of the logarithm of the electric field in the xz plane. Solid black lines indicate the zeros of the electric field. Dashed lines marked as A–C indicate the z -levels of the cross-sections on the three right panels. Panels (A–C) present isoline plots of the logarithm of the electric field and arrow plots of the electric field direction in the xy plane. Solid black lines and black dots mark the points and areas, where the electric field vanishes. Purple arrows indicate the direction of the electric field and serve as guide to the eye. The pulse is at focus ($t=0$) and propagates along the positive z -axis.

of z (see Figure 3A–C). Similarly, the electric field rotates counterclockwise away from the propagation axis.

3 Magnetic field singularities

The magnetic field of the FD pulses presents an even more complex topological behavior than the electric field. In Figure 4, we show the singularities of the modulus of the

magnetic field of the (real) single-cycle pulse, defined as $|\vec{H}_{\rho,z}| = \sqrt{|H_\rho|^2 + |H_z|^2}$, which combines both the radial and longitudinal components. As it can be concluded from Eq. (1), the magnetic field vanishes in 10 different regions on the xz plane, marked by the black dots in Figure 4A. In particular, the magnetic field presents four saddle-like point singularities on the propagation axis (z -axis in Figure 4) with the longitudinal field component pointing toward (away from) and the radial component away from

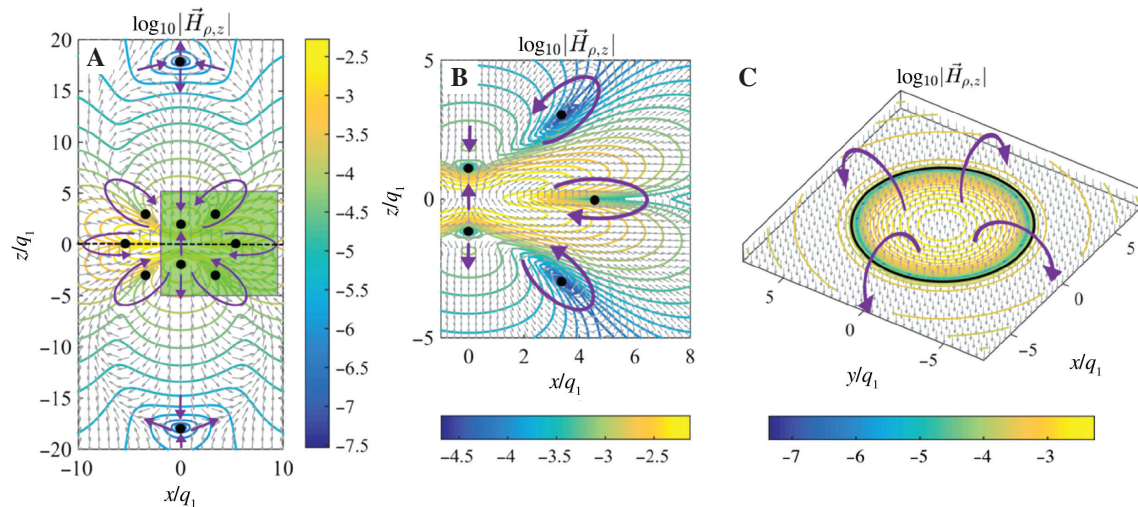


Figure 4: Magnetic field topology of the single-cycle TE FD pulse at focus.

(A, B) Isoline and arrow plot of the logarithm of the magnetic field in the xz plane. Black dots indicate the zeros of the magnetic field. Panel (B) presents a zoom-in of the area highlighted by green in (A). The dashed line in (A) marks the $z=0$ level at which the cross-section presented in (C) is considered. (C) Isoline and arrow plot of the logarithm of the magnetic field in the xy plane at $z=0$ (dashed line in (A)). The magnetic field here vanishes along the circular solid black line. Purple arrows in all panels mark the direction of the magnetic field and serve as guide to the eye. The pulse is at focus ($t=0$) and propagates along the positive z .

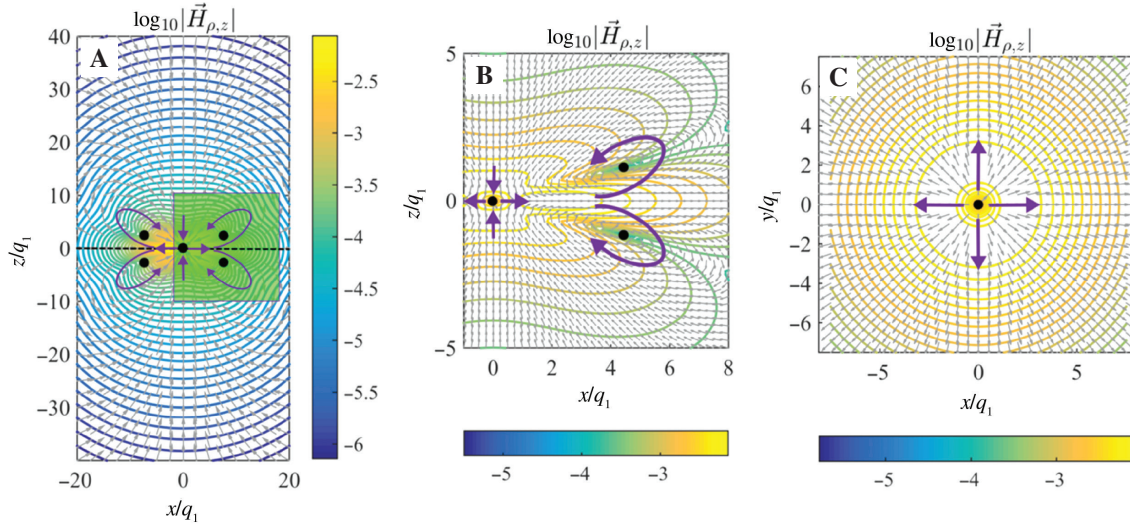


Figure 5: Magnetic field topology of the $1/2$ -cycle TE FD pulse at focus.

(A, B) Isoline and arrow plot of the logarithm of the magnetic field in the xz plane. Black dots indicate the zeros of the magnetic field. Panel (B) presents a zoom-in of the area highlighted by green in (A). The dashed line in (A) marks the $z=0$ level of the cross-sections presented in (C). (C) Isoline and arrow plot of the logarithm of the magnetic field in the xy plane at $z=0$ (dashed line in (A)). The black dot corresponds to the zeros of the magnetic field. Purple arrows in all panels mark the direction of the magnetic field and serve as guide to the eye. The pulse is at focus ($t=0$) and propagates along the positive z .

(toward) the singularity. Away from the propagation axis the magnetic field presents six vortex-like singularities. A zoom-in of the field structure around these singularities can be seen in Figure 4B. For the three off-axis singularities located at the $x > 0$ half space, two of them (at $z > 0$ and $z < 0$) are accompanied by counter-clockwise rotating vortices, whereas the third one (at $z=0$) is accompanied by a clockwise rotating vortex. Owing to the cylindrical symmetry of the pulse, the off-axis singularities in Figure 4A and B correspond in essence to singularity rings. Such an example is shown in Figure 4C, which presents the magnetic field on an xy cross-section at $z=0$. Here, the magnetic field points toward the positive (negative) z -axis inside (outside) the circular region resulting in the formation of a magnetic field vortex winding around the singularity ring. A topological feature of particular interest here is the presence of the on-axis singularities away from the center of the pulse (at $z=0$). Despite these singular points appearing isolated from the rest of the pulse, they are indeed imposed by the spatiotemporal structure at the pulse center and are necessary in order to ensure closed magnetic field lines. Finally, in accordance to the single-cycle duration of the pulse in the electric field, the magnetic field presents $1/2$ cycles.

In the case of the $1/2$ -cycle (imaginary) FD pulse, the magnetic field presents a simpler topological structure with a smaller number of singularities (see Figure 5): one saddle point singularity at the origin ($\rho=0, z=0$) and four

vortices away from the propagation ($\rho=0$) axis. A zoom-in of the latter singularities in the $x > 0$ half-space is shown in Figure 5B. Here, the formation of magnetic field vortices around the singularities can be observed clearly with the vortex at $z > 0$ ($z < 0$) rotating counter-clockwise (clockwise). The field structure around the singularity at $\rho=0, z=0$ reveals a saddle point with the radial component of the magnetic field pointing away from the singularity, while the longitudinal component points toward the singularity (see Figure 5C). In contrast to the (real) single-cycle pulse, here the topological structure of the magnetic field is confined at a region close to the pulse center, while due to the even number of vortex-like regions the on-axis “isolated” singularities are absent.

4 Energy backflow and Poynting vector singularities

The singularities of the electric and magnetic field of the FD pulse lead to a complex topological behavior for the energy flow as represented by the instantaneous Poynting vector (see Figure 6). A striking observation for both the single-cycle (Figure 6A and B) and the $1/2$ -cycle (Figure 6C and D) pulse is the presence of energy backflow (white arrows in Figure 6), a behavior similar to that predicted by Michael Berry for superposition of waves [19], as is

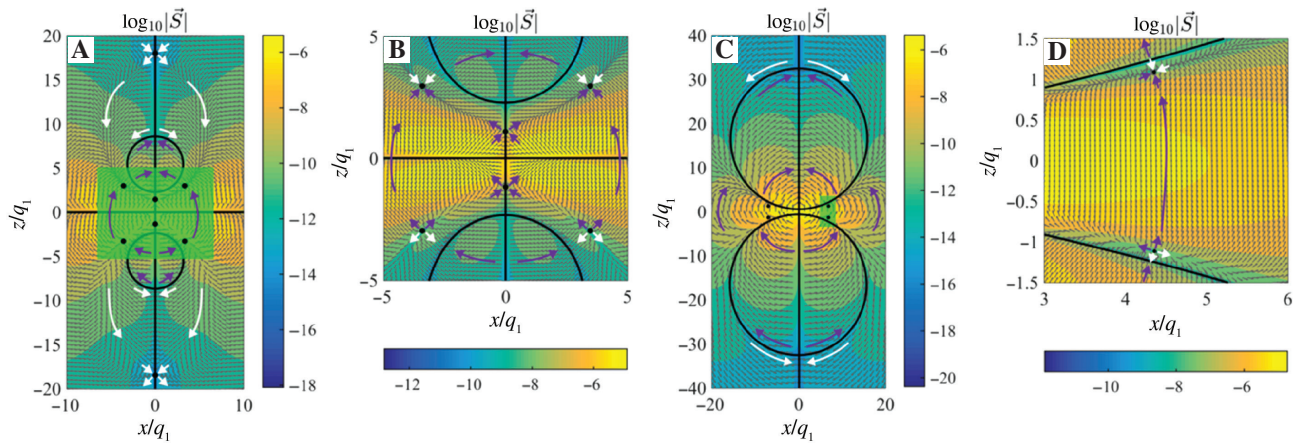


Figure 6: Poynting vector of the TE FD pulse at focus.

Contour and arrow plot of the logarithm of the Poynting vector in the xz plane for the single- (A, B) and $1/2$ -cycle (C, D) pulse. Panels (B) and (D) present zoom-ins of the areas highlighted by green in (A) and (C), respectively. Solid black lines, circles and dots mark the zeros of the Poynting vector. Purple and white arrows indicate areas with forward and backward energy flow, respectively. Note that in regions of backward energy flow, the Poynting vector takes values many orders of magnitude smaller than in the forward flow areas.

the case of superoscillatory light fields [20]. Indeed, the Poynting vector at regions of high intensity is oriented along the propagation direction (parallel to the positive z -axis; see purple arrows in Figure 6), while at regions of relatively low intensity extended energy backflow can be observed (white arrows in Figure 6). In the case of the single-cycle pulse (Figure 6A and B), the Poynting vector vanishes at the positions, where the respective electric and/or magnetic fields are zero. This leads to the vanishing Poynting vector on the xy plane at $z=0$ and along the propagation axis ($\rho=0$). In addition, the Poynting vector vanishes on the two spherical shells around the z -axis, where the electric field is zero (marked by the circular regions in Figure 6A). The Poynting vector also presents four singular points on the z -axis, where both the electric and magnetic fields vanish. All of the on-axis singular points are saddle-like with forward (backward) energy flow close to (away from) the origin. Moreover, the singularities of the Poynting vector include two additional circular regions (indicated as points in Figure 6B) that act as sources and sinks. We would like to note that in contrast to the case of continuous waves, here we are considering the instantaneous energy flow in the pulse, and hence source and sink points have no implications for energy conservation. The Poynting vector for the $1/2$ -cycle pulse presents a very similar topological structure to that of the single-cycle pulse. Indeed, the Poynting vector here also vanishes on the propagation axis due to the azimuthally polarized electric field and on two spherical shells around the z -axis. The main difference compared to the single-cycle pulse is the absence of the singularity plane at $z=0$ and of the saddle point singularities on the z -axis. This is

a direct result of the simpler magnetic field topology of the $1/2$ -cycle FD, which in turn is linked to the temporal shape of the pulse.

5 Conclusions

In summary, we have presented a study of the topological structure of the FD pulse. The availability of analytical expressions for the pulse allows us to examine closely its fine-scale features revealing a large number of singularities in the electric and magnetic fields of various types, including saddle points, vortex lines and rings, planes and spherical surfaces. The field singularities lead to an even more complex topological structure for the instantaneous Poynting vector. Indeed, our results indicate that the FD pulse exhibits extended areas of energy backflow, with the Poynting vector oriented antiparallel to the pulse propagation direction. Nevertheless, this energy backflow is instantaneous and corresponds to areas of very low energy density; hence, the total energy of the pulse still propagates forward. Our analysis has focused on the TE FD pulse, which is azimuthally polarized, but the findings can be readily extended to the radially polarized TM FD by simply exchanging electric and magnetic fields. Although only a single ratio of q_2/q_1 has been considered here, we have observed that by moving closer to the paraxial regime (larger q_2/q_1 ratios) only the location of the singularities changes appreciably but not their type or number. On the other hand, the topology of the pulse experiences dramatic changes upon propagation related to the Gouy

phase shift. An in-depth study of the link between the FD topology and propagation dynamics will be the focus of a future study.

Our findings put forward the FD pulse as an ideal platform to study the instantaneous field singularities of ultrafast vector polarized pulses in both the paraxial and strongly focused regime without resorting to approximations. We anticipate that our results will be relevant to the experimental and theoretical efforts involving the generation, propagation properties and light matter interactions [17, 18, 21–26]. We note that although a part of the fine topological structure in the FD pulse occurs at spatial regions of very low energy, a number of intriguing features manifest close to regions of relatively high energy (e.g. the multiple magnetic field vortices in Figure 4), which can be observed experimentally. Finally, the results presented here suggest that such ultrashort pulses can be employed to study transient phenomena in matter [16, 27–29].

Acknowledgments: The authors acknowledge the support of the MOE Singapore (MOE2016-T3-1-006), the UK's Engineering and Physical Sciences Research Council (grant EP/M009122/1, Funder Id: <http://dx.doi.org/10.13039/501100000266>), the European Research Council (Advanced grant FLEET-786851, Funder Id: <http://dx.doi.org/10.13039/501100000781>), and the Defense Advanced Research Projects Agency (DARPA) under the Nascent Light Matter Interactions program. The data from this paper can be obtained from the University of Southampton ePrints research repository: <https://doi.org/10.5258/SOTON/D0968>.

References

- [1] Batchelor GK. An introduction to fluid-dynamics. Cambridge, Cambridge University Press, 2000.
- [2] Hellwarth RW, Nouchi P. Focused one-cycle electromagnetic pulses. *Phys Rev E* 1996;54:889–95.
- [3] Nye JF, Berry MV. Dislocations in wave trains. *Proc R Soc Lond A* 1974;336:165–90.
- [4] Nye JF. Lines of circular-polarization in electromagnetic-wave fields. *Proc R Soc A* 1983;389:279–90.
- [5] Berry MV. Making waves in physics – three wave singularities from the miraculous 1830s. *Nature* 2000;403:21.
- [6] Dennis MR. Polarization singularities in paraxial vector fields: morphology and statistics. *Opt Commun* 2002;213:201–21.
- [7] Dennis MR, O'Holleran K, Padgett MJ. Singular optics: optical vortices and polarization singularities. *Prog Opt* 2009;53:293–363.
- [8] Freund I. Bichromatic optical Lissajous fields. *Opt Commun* 2003;226:351–76.
- [9] Freund I. Emergent polarization singularities. *Opt Lett* 2004;29:539–41.
- [10] Brittingham JN. Focus waves modes in homogeneous Maxwell equations – transverse electric mode. *J Appl Phys* 1983;54:1179–89.
- [11] Ziolkowski RW. Exact-solutions of the wave-equation with complex source locations. *J Math Phys* 1985;26:861–3.
- [12] Ziolkowski RW. Localized transmission of electromagnetic energy. *Phys Rev A* 1989;39:2005–33.
- [13] Feng SM, Winful HG, Hellwarth RW. Spatiotemporal evolution of focused single-cycle electromagnetic pulses. *Phys Rev E* 1999;59:4630–49.
- [14] Raybould T, Fedotov V, Papasimakis N, Youngs I, Zheludev NI. Focused electromagnetic doughnut pulses and their interaction with interfaces and nanostructures. *Opt Express* 2016;24:3150–61.
- [15] Papasimakis N, Fedotov VA, Savinov V, Raybould TA, Zheludev NI. Electromagnetic toroidal excitations in matter and free space. *Nat Mater* 2016;15:263–71.
- [16] Raybould T, Fedotov VA, Papasimakis N, Youngs I, Zheludev NI. Exciting dynamic anapoles with electromagnetic doughnut pulses. *Appl Phys Lett* 2017;111:081104.
- [17] Papasimakis N, Raybould T, Fedotov VA, Tsai DP, Youngs I, Zheludev NI. Pulse generation scheme for flying electromagnetic doughnuts. *Phys Rev B* 2018;97:201409.
- [18] Zdagkas A, Papasimakis N, Nalla V, Zhang H, Buchnev O, Zheludev NI. Generation of electromagnetic doughnut pulses with a singular metamaterial converter. In: NANOMETA 2019, Seefeld, Austria, 2019.
- [19] Berry MV. Quantum backflow, negative kinetic energy, and optical retro-propagation. *J Phys A: Math Theor* 2010;43:415302.
- [20] Yuan GH, Rogers ETF, Zheludev NI. “Plasmonics” in free space: observation of giant wavevectors, vortices, and energy backflow in superoscillatory optical fields. *Light Sci Appl* 2019;8:2.
- [21] Gbur G, Visser TD, Wolf E. Anomalous behavior of spectra near phase singularities of focused waves. *Phys Rev Lett* 2002;88:013901.
- [22] Popescu G, Dogariu A. Spectral anomalies at wave-front dislocations. *Phys Rev Lett* 2002;88:183902.
- [23] Mariyenko IG, Strohaber J, Uiterwaal CJGJ. Creation of optical vortices in femtosecond pulses. *Opt Express* 2005;13:7599–608.
- [24] Yamane K, Toda Y, Morita R. Ultrashort optical-vortex pulse generation in few-cycle regime. *Opt Express* 2012;20:18986–93.
- [25] Bock M, Brunne J, Treffer A, König S, Wallrabe U, Grunwald R. Sub-3-cycle vortex pulses of tunable topological charge. *Opt Lett* 2013;38:3642–5.
- [26] Kong FQ, Larocque H, Karimi E, Corkum PB, Zhang CM. Generating few-cycle radially polarized pulses. *Optica* 2019;6:160–4.
- [27] Litchinitser NM. Structured light meets structured matter. *Science* 2012;337:1054–5.
- [28] Kim H, Akbarimoosavi M, Feurer T. Probing ultrafast phenomena with radially polarized light. *Appl Opt* 2016;55:4389–94.
- [29] Shigematsu K, Suzuki M, Yamane K, Morita R, Toda Y. Snapshot optical polarization spectroscopy using radially polarized pulses. *Appl Phys Express* 2016;9:122401.